Endoscopic optical coherence tomography of the retina at 1310 nm using paired-angle rotating scanning

Marinko V. Sarunic, Shuo Han, Jigang Wu, Zahid Yaqoob, Mark Humayun, et al.

Marinko V. Sarunic, Shuo Han, Jigang Wu, Zahid Yaqoob, Mark Humayun, Changhuei Yang, "Endoscopic optical coherence tomography of the retina at 1310 nm using paired-angle rotating scanning," Proc. SPIE 6429, Coherence Domain Optical Methods and Optical Coherence Tomography in Biomedicine XI, 642911 (7 February 2007); doi: 10.1117/12.701226

SPIE.

Event: SPIE BiOS, 2007, San Jose, California, United States

Endoscopic Optical Coherence Tomography of the Retina at 1310 nm Using Paired-Angle-Rotating Scanning

Marinko V. Sarunic[1], Shuo Han[2], Jigang Wu[2], Zahid Yaqoob[2], Mark Humayun[3] and Changhuei Yang[2]

1) Engineering Science, Simon Fraser University, Burnaby, BC, V5A 1S6
2) Electrical Engineering, California Institute of Technology, Pasadena, CA 91125
3) Doheny Eye Institute, University of Southern California, Los Angeles, CA 90033.

Vitrectomy (removal of the vitreous humor) is an ophthalmic surgery required as a precursor to several posterior chamber procedures. Vitrectomy is commonly performed using an endoscopic vitreous cutter and fiber based light delivery for observation through a surgical microscope. Cross-sectional visualization of the retina and remnant vitreous layers during surgery using an external optical coherence tomography (OCT) scanner is impractical due to deformation in the shape of the eye and the cornea. We present a forward imaging probe with 820 μm outer diameter (21 gauge needle) for cross-sectional endoscopic OCT imaging during ophthalmic surgeries. The Paired-Angle-Rotating Scanner (PARS) OCT probe is based on angle polished gradient index (GRIN) lenses which are rotated about the optical axis. The scan pattern is determined by the angle between the GRIN lenses and the relative angular velocity. Endoscopic placement of the PARS-OCT probe tip near the retinal surface permits use of a longer wavelength light, in particular 1310 nm, which would otherwise suffer significant attenuation traversing the vitreous humor. The prototype endoscopic PARS-OCT probe is coupled to a commercially available 1310 nm swept laser source, and uses commercial software for data acquisition, processing, and display of retinal images in real time at an A-scan rate of 16 kHz. We present an analysis of aberrations due to off axis use of GRIN lenses and measure the scan pattern of the PARS probe. Images acquired on an *ex vivo* porcine retina are presented, motivating development of the endoscopic PARS-OCT probe for clinical evaluation.

BACKGROUND

Endoscopy enables a clinician to peer through the body's passageways, and has been in existence since the early 1900s [1, 2]. Endoscopy took a great leap forward in 1960s with the introduction of fiber-optic endoscopes [3]. From an operational point of view, a fiber endoscope uses a fiber-optic cable (or a bundle of glass or plastic fibers) to transfer the body cavity images. Fiber endoscopes are usually limited in transverse resolution as they can typically render at most 30,000 resolvable points. This is equivalent to a two-dimensional (2-D) image with 150×200 points. Fiber endoscopes also require the use of additional waveguides or fibers to illuminate the tissue under examination with visible light. Their relatively large diameter limits their usage to wider body passageways such as the GI tract, colon, etc. In addition, these endscopes do not provide depth resolved imaging capability.

An endoscopic imaging modality that can render depth resolved views of the internal tissue structure in the forward region ahead of small diameter probe tip can substantially improve most forms of needle surgical procedures. This can help prevent surgical needles from perforating delicate tissue structures, such as blood vessels and nerves. In the last decade, endoscopic ultrasonography (or endosonography) has been popular among the physicians as it allows

Coherence Domain Optical Methods and Optical Coherence Tomography in Biomedicine XI
edited by James G. Fujimoto, Joseph A. Izatt, Valery V. Tuchin
Proc. of SPIE Vol. 6429, 642911, (2007) · 1605-7422/07/$18 · doi: 10.1117/12.701226

viewing real-time images of intra-abdominal organs. However, owing to the low spatial resolution of endoscopic ultrasound, its accuracy for imaging guided intervention, such as staging a tumor is questionable.

Optical Coherence Tomography (OCT), a non-invasive optical technique for sub-surface tissue imaging, was first developed by Fujimoto's group at MIT about fifteen years ago [4]. The method has since matured into an important clinical imaging modality as it offers numerous advantages: 1) High quality images – OCT has demonstrated the ability to render images to a depth of 1-2 millimeters [5] with 0.5 μm resolution [6]. 2) Flexibility – The light fluence level required for OCT imaging is low enough [7] that OCT can be used in sensitive tissue locales, such as the eye [8-11]. 3) Additional functionality – While a basic OCT imaging method is able to render depth resolved structural images of the target, more sophisticated OCT imaging strategies can provide additional functional information, such as flow (through Doppler OCT) [12, 13], tissue structural arrangement (through birefringence OCT) [14, 15], depth resolved spectral signatures (through spectral OCT) [16, 17], and the spatial distribution of specific contrast agents [18, 19].

In recent years, a new class of OCT techniques called spectral domain (SD) OCT [20] has proven to be a significant improvement over conventional TDOCT in terms of imaging speed and sensitivity [21-23]. SDOCT differs from time domain OCT in that the reference arm is held fixed, and the interferometric signal is acquired over *N* spectral channels, where N commonly varies from ~100 to ~1000. There are two varieties of SDOCT: 1) spectrometer based detection, also known as spectral radar [24] or Fourier domain OCT (FDOCT) [25, 26], which uses a grating to disperse the wavelengths across an arrayed detector, and 2) swept source OCT, also known as optical frequency domain reflectometry (OFDR) [27], wavelength tuning interferometry (WTI) [28], and optical frequency domain imaging (OFDI) [29], which employs a narrowband source rapidly tuned over a broad bandwidth to measure spectral oscillations at evenly spaced wavenumbers.

The system topology of a swept source SDOCT scheme is shown in Figure 1. Light is split into two components by the 2x2 fiber coupler. One component is directed at the sample, and the other is sent to a reference mirror. The back-scattered sample and back-reflected reference signals are then re-channeled and combined through the same coupler, generating interferometric fringes superimposed on the spectral profile of the source. A circulator in the source arm permits balanced detection for improved sensitivity. The locations of scatterers in the sample are encoded by the frequency of interferometric fringes. Performing the Fourier transform on the interferogram generates an A-scan which represents a linear cross-sectional reflectivity profile through the sample.

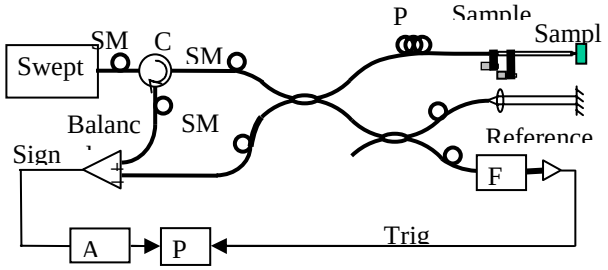

Figure 1. Schematic of the swept source OCT system with PARS-OCT probe. SMF: single-mode fiber; C: circulator; P: polarization controller; ADC: analog-to-digital converter; PC: personal computer; FP: Fabry-Perot cavity.

Mathematically, the spectrally resolved signal can be written as:

$$P_{detector}(k,\Delta k,z) = 2\sqrt{P_{Ro}P_{So}}\,S(\Delta k)\,e^{-\int_0^{x_s}[\mu_a(\lambda,x_s')+\mu_s(\lambda,x_s')]dx_s'}\sqrt{R(\lambda,x_s)}\cos[2\pi(k+\Delta k)(z-x_s)], \qquad (1)$$

where Δk is the wavenumber difference from the center wavenumber *k*, $S(\Delta k)$ is source's spectral profile, P_{Ro} is the collected reference arm power, P_{So} is the collected signal arm power if the sample is fully reflective, $R(\lambda, x_s)$ is the sample reflectivity at depth x_s, and *z* is the depth into the sample. The additional exponential term accounts for the loss of collected light due to absorption and scattering during the passage into and out of the sample. Notice that the period of the spectral oscillation of the measured signal in *k*-space is proportional to $(z - x_s)$. Also notice that in SDOCT detection, signal contribution from two or more interfaces may be collected simultaneously as they contribute to different

spectral oscillation frequencies. In other words, signal from each location $(z - x_s)$ can be detected over the entire measurement time *T*.

Several OCT based endoscopic systems have been implemented over the past decade. Multiple imaging studies have been conducted within different organ systems, including the GI tract [30, 31], bladder tumors [32], and the atherosclerotic walls of coronary arteries [33, 34], and monitoring intracoronary stenting [35]. The primary design consideration here is to minimize the diameter of the OCT probe. To this end, the single mode fiber used for light transmission in most OCT systems is ideally suited for the purpose. OCT imaging needle/catheter can be categorized into 2 major classes – side imaging and forward imaging.

Most of the OCT endoscope/catheter systems reported in the literature are circumferential or side-scanning systems suitable for circumferential imaging of the immediate environment [36-40]. In these systems, the OCT probe light is emitted from and collected at the side of the probe. The general design of such a probe consists of using a rod mirror or prism attached to a rotation assembly to deflect the emitted light from the optical fiber tip out of a window on the side of the probe. By rotating the probe orientation rapidly, a cross-sectional (basically 2-D with depth perception) view of the tissue can be generated. The size of reported side imaging OCT probes (referenced above) varies from 0.4 to 5 mm, depending upon the rotation assembly employed.

Forward imaging OCT endoscopic systems can be very useful in providing tissue structural information in front of the catheter probe or surgical needle for the purpose of surgical guidance or image-guided device placement. Unlike side imaging OCT systems, the implementation of forward imaging systems with a narrow probe poses very significant technological challenges. The first forward-imaging probes for OCT were reported by Boppart et al. [41]. In particular, two probe designs were proposed and demonstrated; both used a 6.4 mm diameter lead zirconate titanate (PZT) cantilever for mechanical scanning. In one design [see Figure 2 (a)], the PZT cantilever was used to translate a fiber and a GRIN lens together for output beam scanning. Although, the fiber-GRIN lens assembly itself was compact, the overall size of the forward-imaging instrument was significant mainly due to large diameter of the PZT cantilever. In the other design, shown in Figure 2 (b), the fiber-GRIN lens assembly was translated in the image plane of a long (19.5 cm) rod lens to realize a rigid forward-imaging OCT probe for laparoscopic procedures. Recently, Xie et al. [42] employed a similar scheme with a SDOCT system to perform in vivo imaging with dynamic focusing capability. The diameters of the GRIN lenses used in this case were 2.7 mm and 4.6 mm respectively.

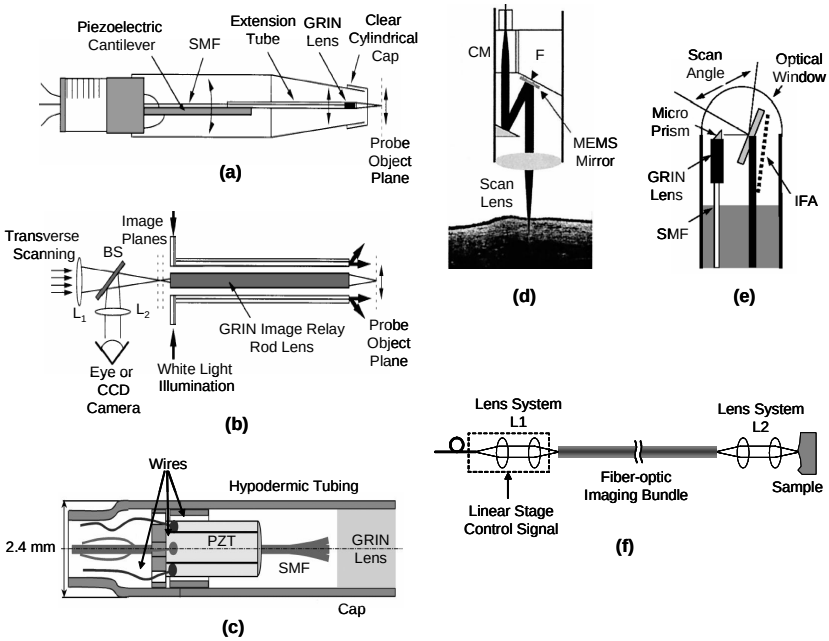

Figure 2 Forward-imaging OCT probes. (a) Hand-held OCT probe. (b) Rigid OCT laparoscope for minimally invasive procedures. (c) Flexible rapid scanning miniature OCT endoscope. (d) Schematic of MEMS-based OCT endoscope, where (e) shows a MEMS mirror with pivot point in the middle of the mirror. (f) Fiber-bundle based OCT endoscope design.

In 2004, Liu et al. [43] demonstrated the use of a smaller (1.5 mm) diameter PZT actuator to oscillate position of a fiber in front of a stationary GRIN lens for output beam scanning [see Figure 2 (c)]. The overall size of probe was 2.4 mm with lateral scan range of 2.5 mm. This method has the advantage of rapid scanning due to the PZT scanner.

Another class of forward-imaging probes has reported the use of micro-electro-mechanical systems (MEMS) based mirrors at the distal end for output beam scanning. Typically, light from the sample arm fiber is collimated before it enters into a beam folding optics, with one element as a MEMS-based scanning mirror; the scanning optical beam is then focused by a scan lens. Two such OCT endoscopes have reported the use of flapping MEMS mirrors, with a bimorph thermally actuated contraction hinge at one end [44, 45]. The MEMS-based endoscopes were 5 mm in diameter, with lateral scan range of 2.9 mm [44] and 4.3 mm [45]. In comparison, Zara et al. [46] have also reported a MEMS scanner, with pivot point in the middle of the mirror, for endoscopic OCT; an integrated force array (IFA) linear actuator attached at one end of the mirror was used to pull and tilt the mirror for beam scanning [see Figure 2 (e)]. The MEMS mirror was incorporated into an OCT system for proof-of-concept demonstration; however, the scanner requires modification and appropriate packaging prior to use in endoscopic applications [46].

In addition, a 2-axis MEMS mirrors at the distal end can also be used to acquire forward OCT images [47]. In this respect, Yeow et al. have reported proof-of-concept 3-D or volumetric OCT imaging of a fruit fly using of a 2-D MEMS scanner actuated by electrostatic forces [48]. Another noteworthy effort in this direction reports the use of a 2-D MEMS mirror for forward volumetric OCT imaging of hamster cheek [49]. However, further technology development is required to incorporate the scanner into an OCT probe for endoscopic applications. We also note that the MEMS-based probes are generally large in size, limiting their application to relatively large body passageways. Recently, one approach to forward volumetric OCT imaging has reported the use of 2-D beam scanning at the proximal end of a fiber-bundle [see Figure 2 (f)]; a unity magnification lens-imaging system at the distal end was employed to focus the probe beam on the tissue sample [50]. The fiber-bundle-based OCT endoscope was 3.2 mm in diameter, with a 2.8 mm working distance.

Despite the extensive amount of research that has been invested in forward imaging OCT probes thus far, a forward OCT imaging probe that is small enough (20 gauge or higher) for use in needle surgical procedures has yet to be developed. The reasons are varied. A number of research groups are focused on body passageways imaging applications where a small probe is not required. More importantly, most of technologies that we have discussed are simply not suitable for miniaturization to the desired scale. The probe design proposed here is easy to miniaturize. We expect to build a 21 gauge probe in the immediate future.

The forward imaging OCT based needle probe system proposed in this grant application will greatly benefit a very wide range of image guided interventional procedures by providing a pilot view perspective straight from the tip of the needle. Such kind of image guidance should have a very significant impact in reducing surgical errors and improving surgical accuracy. As a starting point, we highlight the specific application of the probe in retinal imaging during vitreoretinal surgery.

VITREORETINAL SURGERY

Optical coherence tomography has already generated a significant impact to diagnostic ophthalmology, particularly in retinal imaging. Carl Zeiss Meditec has successfully commercialized a time domain OCT retinal scanner (StratusOCT) which is integrated into a slit lamp biomicroscope to facilitate patient alignment and imaging in a clinical setting. Laboratory based state of the art Fourier domain OCT retinal imagers provide scan rates up to 30 kHz [51] (nearly two orders of magnitude faster than time domain systems), but their development has also been limited to slit-lamp based configurations [52-54]. These systems typically operate at a central wavelength of 830nm to minimize absorption incurred traversing the vitreous humor (a penalty of 21 dB in sensitivity is observed at 1310nm [55]). Slit lamp based retinal imagers scan the surface of the cornea with a collimated beam, relying on refraction through the cornea and crystalline lens to focus the beam on the retina. Accordingly, these systems are not compatible with surgical procedures wherein the vitreous humor has been compromised, or the corneal surface is deformed.

Vitrectomy surgery (removal of the vitreous humor) is an ophthalmic surgery required for correction of common pathologies such as: retinal detachment due to complications in diabetic retinopathy, macular holes, and vitreous hemorrhaging. Vitrectomy is commonly performed using endoscopic instruments inserted through incisions in the sclera made at the pars plana, just behind the iris and crystalline lens. Presently, no tool is available for cross sectional imaging of the retinal layers during surgery or to assist in visualization of remnant vitreous layers on the retina. The complete removal of the vitreous during vitrectomy is extremely important for a successful procedure, and dyes are often used to stain remnants of the vitreous clinging to the retina introducing issues of dye removal and toxicity.

Paired-Angle-Rotating Scanner (PARS) OCT presents an excellent forward imaging endoscopic tool for use during vitreoretinal surgery. The small diameter of the PARS-OCT probe permits access to the retinal via small incisions in the sclera commonly used during vitrectomy for insertion of the vitrector, illumination fiber, and other endoscopic tools. Situation of the PARS-OCT probe tip near the retinal surface will provide cross sectional images of the retinal layers familiar from external retinal scanners, including the retinal nerve fiber layer, ganglion cell/inner plexiform layer, inner nuclear layer, outer plexiform layer, outer nuclear layer, and the inner/outer segment junction. Additionally, due to the proximity of the probe to the retinal surface during surgery, the center wavelength of the PARS-OCT system is not limited by absorption through the vitreous. The use of longer wavelengths, particularly in the 1300 nm region, can significantly improve visibility of choriocapillaries and the choroid compared to imaging at 1050nm and 830nm, as demonstrated in the literature for *ex vivo* porcine retinas [55].

In this report we discuss a forward imaging endoscopic OCT probe designed to provide surgeons with real time cross-sectional imaging of the retina during surgery. Unlike side-imaging probes, which acquire planar images as the interrogating beam is rotated, a forward imaging probe requires a scanning mechanism to visualize the area directly in front of the probe tip. A forward imaging endoscopic probe for imaging the retina is sketched in Figure 3. The probe can be inserted through a cannulated incision in the eye at the pars plana, in a procedure similar to that performed during endoscopic vitrectomy. The lateral position of the beam is achieved using PARS. [56] This particular application area is extremely well suited for our initial evaluation of the probe technique in clinical applications for two main reasons. First, OCT is an established ophthalmology technique – the extensive body of work can inform and guide our research application. Second, tissue trauma will be absent – we can fully evaluate the utility of the probe's performance without having to contend with any potential trauma associated artifacts. With the knowledge gained about the probe's performance, we will be better able to tackle potential trauma associated artifacts in future applications.

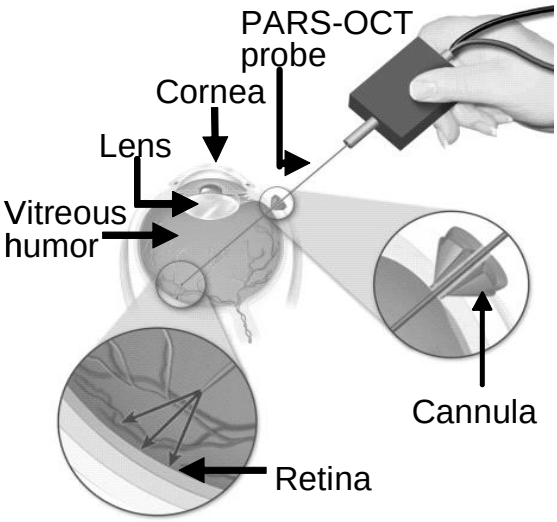

Figure 3 Forward imaging PARS-OCT endoscope for retinal examination though an incision at the pars plana.

PARS OCT

The PARS-OCT probe utilizes two angle polished GRIN lenses which are rotated about the optical axis to steer the beam position.[56] As sketched in Figure 4, the GRIN lenses are encased in two concentric needles which may be spun independently. The inner faces of the GRIN lenses are polished at identical angles, and separated by a controlled air gap. The first GRIN lens is slightly longer than ¼ pitch, producing a slightly converging beam between the lenses. Refraction at the first angle polished surface directs the beam off axis to the second GRIN lens. The length of the second GRIN lens determines focal distance, thus the length is less than ¼ pitch. The beam continues off axis in the second GRIN lens, and is again refracted as it exits through the flat polished surface. Controlling the angle of the GRIN lenses with respect to each other determines the scan pattern as illustrated in Figure 4 (b) and (c).

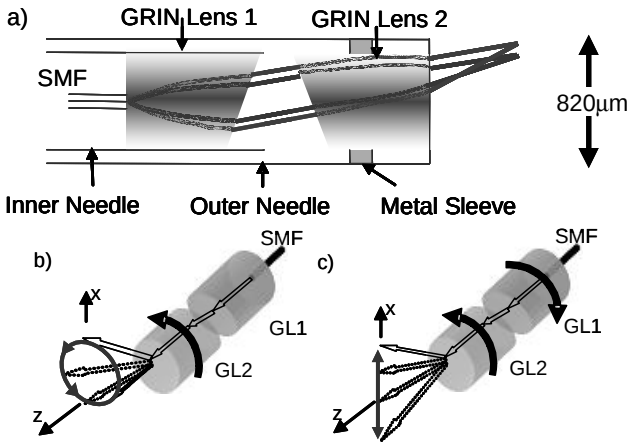

Figure 4 (a) The PARS-OCT probe consists of two angle polished GRIN lenses. (b) Holding GL1 stationary, and rotating GL2 produces a circular scan (c) Rotating both GL1 and GL2 in opposite directions produces a linear scan which retraces itself after 180^{o} of rotation.

The PARS-OCT probe requires off-axis beam propagation in GRIN lenses, potentially introducing signification image artifact. In particular, chromatic based aberrations are anticipated due to the use of a spectrally broad source. In the standard chromatic aberration, the wavelength dependent refractive index causes different wavelengths to focus at slightly different axial locations. In standard systems, this is typically addressed by the use of achromatic doublet lenses, but is not easily addressed using GRIN lenses. Additionally, an off axis aberration unique to the PARS-OCT probe occurs due to the dispersive effects of the internal angle polished surfaces, as illustrated in Figure 4 (a). Due to the dependence of refractive index on wavelength, Snell's Law refraction will cause different wavelengths will focus at slightly different lateral positions, The broadening of the focal spot increases with increasing scan angle, and is a major design concern for the probe.

We are developing a detailed ZEMAX model to determine the maximum angles permitted for the GRIN lenses and the effects to the spot shape. The model is based on GRIN lenses of 500 µm outer diameter, using the refractive index gradient and glass dispersion coefficients obtained from the lens supplier (GRINTech, GmbH). Due to the short length and small diameter the second lens, an additional ½ pitch was added to the overall length to facilitate manufacturability. For an internal angle of 15^{o}, and a working distance of 2 mm, we expect a scan arc length of 1.1 mm

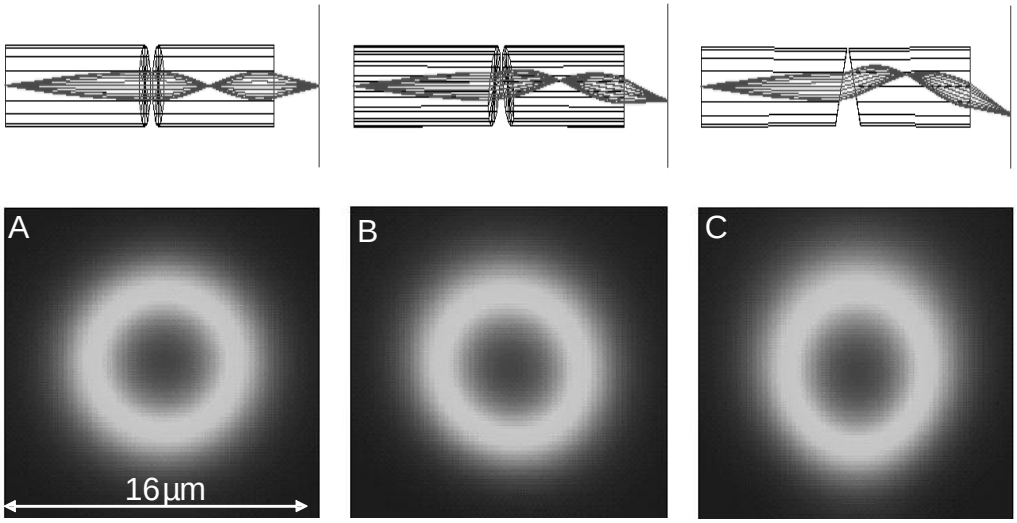

Figure 5 Zemax model results for the point spread function of the PARS-OCT probe at the following locations (a) axial, (b) half maximum deflection (c) maximum deflection.

and thus effective numerical aperture of N.A. = 0.1. The results, shown in Figure 5 for on-axis and off-axis scan locations, indicate that the point spread function is not severely degraded, and that minimal distortion in the beam circularity is expected even for the most deflected beam.

PROTOTYPE PROBES

The first report using PARS-OCT was performed using a probe with an outer of 1.65 mm, and a fixed platform with bulky motors for imaging *Xenopus laevis* tadpoles.[56] However, the PARS-OCT design is scalable, and readily lends itself to miniaturization. In this report we present a prototype, hand-held PARS-OCT probe with rotating angle polished GRIN lenses housed in a 21 gauge needle, providing a outer diameter of 820 μm. The GRIN lenses are 500 μm in diameter, polished at a 15^{o} angle, and provide a working distance of 1 mm. The actuation system for rotating the inner and outer needles to perform scans consists of a fiber rotary joint, a pair of lightweight servo motors with custom encoders and associated gears, as sketched in Figure 6 (a), and photographed in Figure 6 (b). For this summary, the inner probe (corresponding to the first GRIN lens) was held stationary and only the outer probe tip (the second GRIN lens) was rotated, resulting in a circular scan pattern as sketched in Figure 4 (b). The measured scan pattern is shown in Figure 6 (c), acquired using a 632 nm laser with the PARS-OCT probe tip suspended above a planar CCD imager.

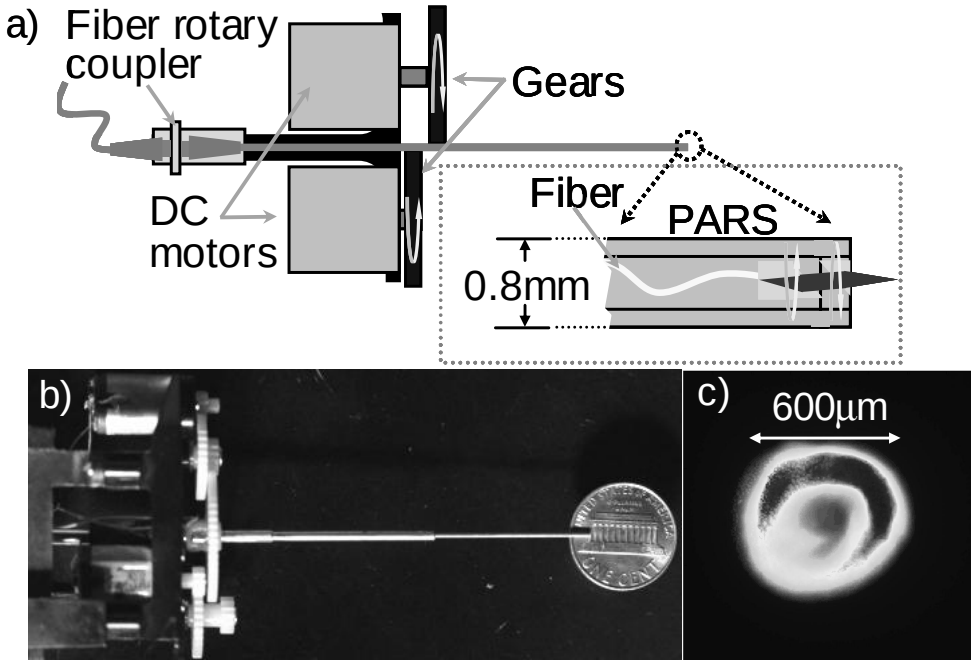

Figure 6 a) Sketch of the hand held PARS-OCT probe. b) Photo of the 0.82 mm diameter probe with motor and gears next to a penny. c) Circular scan pattern obtained while rotating only the second GRIN lens (outer needle housing).

The PARS-OCT probe is compatible with any center wavelength, and for optimal tissue penetration, this prototype was designed for 1310 nm. Due to the near proximity of the PARS-OCT probe to the retina attenuation of the optical beam through the vitreous attenuation is minimal, permitting the use of longer wavelength illumination. A central wavelength of 1310 nm is desirable due to the improved visibility of the choroid and choriocapillaries over 830 nm and 1050 nm, as previously reported in the literature using excised porcine retinas. [55] An additional benefit of using 1310nm illumination with the PARS-OCT probe is that the higher absorption by the vitreous humor is expected to improve visualization of remnant vitreous adhering to the retina.

Capitalizing on the inherent sensitivity advantage of Fourier domain systems, a commercially available swept laser was selected as the source illumination (Thorlabs, λ_o = 1310 nm, $\Delta\lambda$ = 110nm, 16 kHz) [57]. The Thorlabs software operates in real time, including resampling of the spectral interferogram to be evenly spaced in wavenumber. The displayed frame rate is dependent on the user adjustable number of A-scan per B-scan.

In a preliminary study, the PARS-OCT probe photographed in Figure 6 (b) was used to image the retina of an enucleated porcine eye with cornea, lens, and vitreous removed. The power at the sample was 2.3 mW, and balanced detection was used. Each B-scan consisted of 1984 A-scans, displayed at a rate of 6.9 frames per second. The angular velocity of the PARS-OCT probe and frame rate of the acquisition were matched using custom software. In the resulting images, shown in Figure 7, a remnant vitreous layer was clearly observed (surface rippled due to vibration at the probe tip). Blood vessels in the optic nerve head, and choroicapillaries were obsereved. The characteristic retinal layers are not observed due to deterioration of the retina in *ex vivo* tissue, and lack of numerical dispersion compensation.

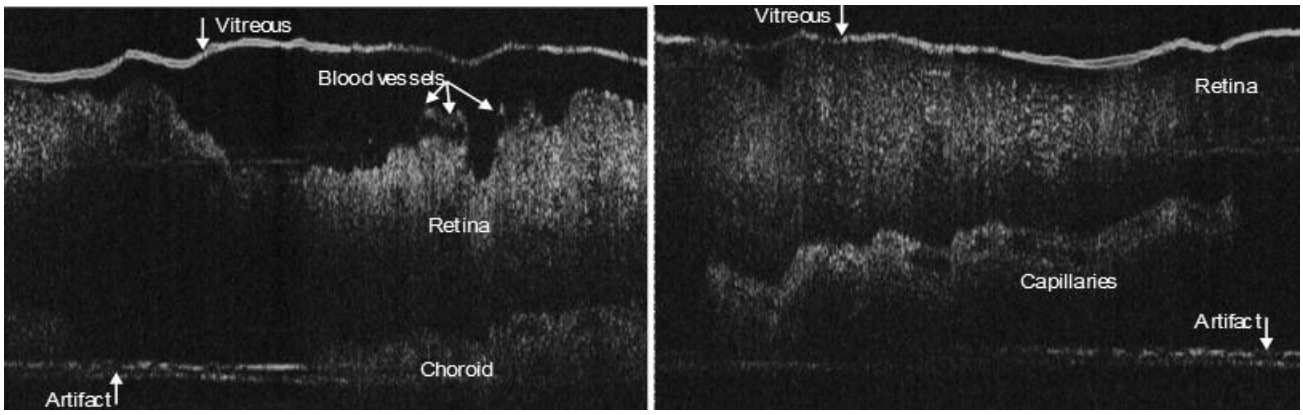

Figure 7 Images of ex vivo porcine retina acquired with the PARS-OCT probe using a circular scan as sketched in Figure 4 (a). A bright reflection is observed from remnant vitreous layers. The left panel was acquired near the optic nerve head. The vertical depth of each image is 2.3mm, and the width (circumferential distance) is ~2.5mm.

LINEAR SCAN PROBE

The probe described above permits arbitrary control of the rotational speed of the inner and outer GRIN lenses in the PARS tips. Although this permits development of three dimensional scan patterns (spiral, starburst, etc), the required control circuitry and mechanisms pose unnecessary complications for simple linear scanning applications. For this reason, a second generation probe exclusively for linear scans has been developed making use of mechanical gearing in place of control electronics. The gear-based linear drive chassis, illustrated in Figure 8, uses only a single lightweight motor to drive both PARS lenses at the same rotation speed in opposite directions, and is compatible with the probe tips developed for the two-motor design.

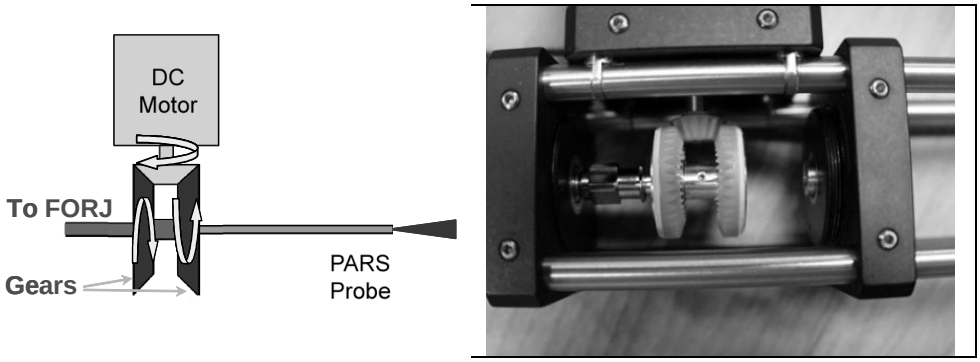

Figure 8 (a) Schematic and (b) photograph of the mechanically linked counter rotation system used to obtain a linear scan using PARS-OCT.

The linear-scan chassis was also used to investigate imaging of the vitreo-retinal layers in enucleated porcine eyes after vitrectomy. The optical source used for these measurements was a Micron Optics Swept Laser which operated at a sweep rate of 250 Hz. The results in Figure 9 demonstrate clear visualization of the remnant vitreous surface, retinal layers, and the choroid.

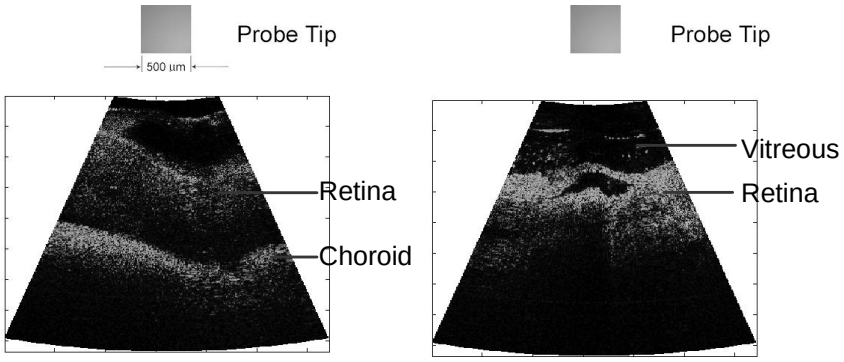

Figure 9 Illustration of the OCT endoscopic inspection of the retina using the linear-scanning probe of ex vivo porcine eye showing (left) posterior segment and (right) retinal detachment.

SUMMARY

Endoscopic retinal imaging may facilitate ocular posterior chamber procedures such as vitrectomy, removal of the vitreous humor. We have developed a forward imaging probe which provides beam scanning at the image plane using angle polished GRIN lenses. The optics were housed in 21 gauge hypodermic needle, providing an 820 micron outer diameter for minimally invasive procedures. Promising results obtained with the probe for imaging the retina of ex vivo porcine eyes encourage further development leading to development of a tool for clinical use.

REFERENCES

1. Kelling, G., *Endoscopy of the oesophagus and stomach.* Lancet, 1900. 1: p. 1189-1198.
2. Killian, G., On direct endoscopy of the upper air passages and oesophagus : Its diagnostic and therapeutic value in the search for and removal of foreign bodies. British Medical Journal, 1902. 1902: p. 569-571.
3. Wallace, F.J., *Fiber Optic Endoscopy.* Journal of Urology, 1963. 90(3): p. 324-&.
4. Huang, D., et al., *Optical Coherence Tomography.* Science, 1991. 254: p. 1178-1181.
5. Schmitt, J.M., S.L. Lee, and K.M. Yung, *An optical coherence microscope with enhanced resolving power in thick tissue.* Optics Communications, 1997. 142(4-6): p. 203-207.
6. Povazay, B., et al., *Submicrometer axial resolution optical coherence tomography.* Optics Letters, 2002. 27(20): p. 1800-1802.
7. American_National_Standards_Institute, *Safe Use of Lasers*, in *ANSI Z 136*. 2000, Laser Institute of America: Orlando, Florida. p. 1-2000.
8. Swanson, E.A., et al., *In-Vivo Retinal Imaging by Optical Coherence Tomography.* Optics Letters, 1993. 18(21): p. 1864-1866.
9. Izatt, J.A., et al., *High-Speed in-Vivo Retinal Imaging with Optical Coherence Tomography.* Investigative Ophthalmology & Visual Science, 1994. 35(4): p. 1729-1729.
10. Hee, M.R., et al., *Optical Coherence Tomography of the Human Retina.* Archives of Ophthalmology, 1995. 113(3): p. 325-332.
11. Podoleanu, A.G., et al., Simultaneous en-face imaging of two layers in the human retina by low-coherence reflectometry. Optics Letters, 1997. 22(13): p. 1039-1041.
12. Izatt, J.A., et al., In vivo bi-directional color Doppler flow imaging of picoliter blood volumes using optical coherence tomography. Optics Letters, 1997. 22: p. 4139-4141.
13. Yazdanfar, S., A.M. Rollins, and J.A. Izatt, Imaging and velocimetry of the human retinal circulation with color Doppler optical coherence tomography. Optics Letters, 2000. 25(19): p. 1448-1450.
14. deBoer, J.F., et al., Two-dimensional birefringence imaging in biological tissue by polarization-sensitive optical coherence tomography. Optics Letters, 1997. 22(12): p. 934-936.
15. Everett, M.J., et al., Birefringence characterization of biological tissue by use of optical coherence tomography. Optics Letters, 1998. 23(3): p. 228-230.
16. Morgner, U., et al., *Spectroscopic optical coherence tomography.* Optics Letters, 2000. 25(2): p. 111-113.

17. Leitgeb, R., et al., Spectral measurement of absorption by spectroscopic frequency-domain optical coherence tomography. Optics Letters, 2000. 25(11): p. 820 - 822.
18. Rao, K.D., et al., Molecular contrast in optical coherence tomography by use of a pump-probe technique. Optics Letters, 2003. 28(5): p. 340-342.
19. Yang, C.H., *Molecular Contrast Optical Coherence Tomography: A Review.* Photochemistry and Photobiology, 2005. 81: p. 215-237.
20. Fercher, A.F., et al., Measurement of Intraocular Distances by Backscattering Spectral Interferometry. Optics Communications, 1995. 117(1-2): p. 43-48.
21. Choma, M.A., et al., Sensitivity advantage of swept source and Fourier domain optical coherence tomography. Optics Express, 2003. 11(18): p. 2183 - 2189.
22. de Boer, J.F., et al., Improved signal-to-noise ratio in spectral-domain compared with time-domain optical coherence tomography. Optics Letters, 2003. 28(21): p. 2067 -2069.
23. Leitgeb, R., C.K. Hitzenberger, and A.F. Fercher, *Performance of fourier domain vs. time domain optical coherence tomography.* Optics Express, 2003. 11(8): p. 889-894.
24. Hausler, G. and M.W. Lindner, *"Coherence Radar" and "Spectral Radar" - New Tools for Dermatological Diagnosis.* Journal of Biomedical Optics, 1998. 3: p. 21.
25. Wojtkowski, M., et al., *In vivo human retinal imaging by Fourier domain optical coherence tomography.* Journal of Biomedical Optics, 2002. 7(3): p. 457-463.
26. Wojtkowski, M., et al., Ultrahigh-resolution, high-speed, Fourier domain optical coherence tomography and methods for dispersion compensation. Optics Express, 2004. 12: p. 2404.
27. Golubovic, B., et al., Optical frequency-domain reflectometry using rapid wavelength tuning of a Cr4+:forsterite laser. Optics Letters, 1997. 22(22): p. 1704-1706.
28. Lexer, F., et al., *Wavelength-tuning interferometry of intraocular distances.* Applied Optics-OT, 1997. 36(25): p. 6548-6553.
29. Yun, S.H., et al., *High-speed optical frequency-domain imaging.* Optics Express, 2003. 11(22): p. 2953-2963.
30. Rollins, A.M., et al., Real-time in vivo imaging of human gastrointestinal ultrastructure by use of endoscopic optical coherence tomography with a novel efficient interferometer design. Optics Letters, 1999. 24(19): p. 1358-1360.
31. Sivak, M.V., et al., High-resolution endoscopic imaging of the GI tract using optical coherence tomography. Gastrointestinal Endoscopy, 2000. 51(4): p. 474-479.
32. Xie, T.Q., M.L. Zeidel, and Y. Pan, Detection of tumorigenesis in urinary bladder with optical coherence tomography: optical characterization of morphological changes, in Optics express. 2002. p. 1431-1443.
33. Tearney, G. and B. Bouma, Atherosclerotic plaque characterization by spatial and temporal speckle pattern analysis. Optics Letters, 2002. 27(7): p. 533 -535.
34. Yabushita, H., et al., Monitoring atherosclerotic plaque evolution in vivo by optical coherence tomography. Circulation, 2003. 108(17): p. 416.
35. Bouma, B.E., et al., Evaluation of intracoronary stenting by intravascular optical coherence tomography. Heart, 2003. 89(3): p. 317-320.
36. Herz, P.R., et al., Micromotor endoscope catheter for in vivo, ultrahigh-resolution optical coherence tomography. Optics Letters, 2004. 29(19): p. 2261-2263.
37. Tearney, G.J., et al., Scanning single-mode fiber optic catheter-endoscope for optical coherence tomography. Optics Letters, 1996. 21(7): p. 543-545.
38. Tearney, G., et al., In vivo endoscopic optical biopsy with optical coherence tomography. Science, 1997. 276(5321): p. 2037-2039.
39. Yang, V.X.D., et al., High speed, wide velocity dynamic range Doppler optical coherence tomography (Part III): in vivo endoscopic imaging of blood flow in the rat and human gastrointestinal tracts. Optics Express, 2003. 11(19): p. 2416-2424.
40. Tumlinson, A.R., et al., Miniature endoscope for simultaneous optical coherence tomography and laser-induced fluorescence measurement. Applied Optics, 2004. 43(1): p. 113-121.
41. Boppart, S.A., et al., *Forward-imaging instruments for optical coherence tomography.* Optics Letters, 1997. 22(21): p. 1618-1620.
42. Xie, T.Q., et al., GRIN lens rod based probe for endoscopic spectral domain optical coherence tomography with fast dynamic focus tracking. Optics Express, 2006. 14(8): p. 3238-3246.
43. Liu, X.M., et al., Rapid-scanning forward-imaging miniature endoscope for real-time optical coherence tomography. Optics Letters, 2004. 29(15): p. 1763-1765.

44. Pan, Y.T., H.K. Xie, and G.K. Fedder, *Endoscopic optical coherence tomography based on a microelectromechanical mirror.* Optics Letters, 2001. 26(24): p. 1966-1968.
45. Xie, T.Q., et al., Endoscopic optical coherence tomography with a modified microelectromechanical systems mirror for detection of bladder cancers. Applied Optics, 2003. 42(31): p. 6422-6426.
46. Zara, J.M., et al., Electrostatic micromachine scanning mirror for optical coherence tomography. Opt. Lett., 2003. 28: p. 628--630.
47. Jain, A., et al., *A two-axis electrothermal micromirror for endoscopic optical coherence tomography.* Ieee Journal of Selected Topics in Quantum Electronics, 2004. 10(3): p. 636-642.
48. Yeow, J.T.W., et al., *Micromachined 2-D scanner for 3-D optical coherence tomography.* Sensors and Actuators a-Physical, 2005. 117(2): p. 331-340.
49. Hanna, N., et al., Two-dimensonal and 3-dimensional optical coherence tomographic imaging of the airway, lung, and pleura. Journal of Thoracic and Cardiovascular Surgery, 2005. 129(3): p. 615-622.
50. Xie, T.Q., et al., *Fiber-optic-bundle-based optical coherence tomography.* Optics Letters, 2005. 30(14): p. 1803-1805.
51. Cense, B. and N.A. Nassif, Ultrahigh-resolution high-speed retinal imaging using spectral-domain optical coherence tomography. Optics Express, 2004. 12(11): p. 2435-2447.
52. Cense, B., et al., Ultrahigh-resolution high-speed retinal imaging using spectral-domain optical coherence tomography Optics Express, 2004. 12(11): p. 2435-2447.
53. Leitgeb, R.A., et al., *Ultrahigh resolution Fourier domain optical coherence tomography.* Optics Express, 2004. 12(10): p. 2156-2165.
54. Wojtkowski, M., et al., Ultrahigh-resolution, high-speed, Fourier domain optical coherence tomography and methods for dispersion compensation. Optics Express, 2004. 12(11): p. 2404-2422.
55. Povazay, B., et al., Enhanced visualization of choroidal vessels using ultrahigh resolution ophthalmic OCT at 1050 nm. Optics Express, 2003. 11(17): p. 1980-1986.
56. Wu, J., et al., Paired-angle-rotation scanning optical coherence tomography forward-imaging probe. Optics Letters, 2006. 31(9): p. 1265-67.
57. Huber, R., et al., Three-dimensional and C-mode OCT imaging with a compact, frequency swept laser source at 1300 nm. Optics Express, 2005. 13: p. 10523-10538